PAPER

The role of extended range of interactions in the dynamics of interacting molecular motors

To cite this article: Cade Spaulding et al 2022 J. Phys. A: Math. Theor. 55 255601

View the article online for updates and enhancements.

You may also like

- Theoretical analysis of dynamic processes for interacting molecular motors
 Hamid Teimouri, Anatoly B Kolomeisky and Kareem Mehrabiani
- The role of dynamic defects in transport of interacting molecular motors
 Akriti Jindal, Anatoly B Kolomeisky and Arvind Kumar Gupta
- <u>Van der Waals interactions in advanced</u> <u>materials, in memory of David C Langreth</u> Martin Weinelt and Felix von Oppen



IOP ebooks™

Bringing together innovative digital publishing with leading authors from the global scientific community.

Start exploring the collection-download the first chapter of every title for free.

The role of extended range of interactions in the dynamics of interacting molecular motors

Cade Spaulding^{1,2,*}, Hamid Teimouri^{1,2,*}, S L Narasimhan³ and Anatoly B Kolomeisky^{1,2,4,5,**}

- Department of Chemistry, Rice University, Houston, TX 77005, United States of America
- ² Center for Theoretical Biological Physics, Rice University, Houston, TX 77005, United States of America
- ³ Chennai Mathematical Institute, SIPCOT IT Park, Siruseri 603103, India
- ⁴ Department of Chemical and Biomolecular Engineering, Rice University, Houston, TX 77005, United States of America
- Department of Physics and Astronomy, Rice University, Houston, TX 77005, United States of America

E-mail: tolya@rice.edu

Received 27 December 2021, revised 14 April 2022 Accepted for publication 17 May 2022 Published 6 June 2022



Abstract

Motor proteins, also known as biological molecular motors, play important roles in various intracellular processes. Experimental investigations suggest that molecular motors interact with each other during the cellular transport, but the nature of such interactions remains not well understood. Stimulated by these observations, we present a theoretical study aimed to understand the effect of the range of interactions on dynamics of interacting molecular motors. For this purpose, we develop a new version of the totally asymmetric simple exclusion processes in which nearest-neighbor as well as the next nearest-neighbor interactions are taken into account in a thermodynamically consistent way. A theoretical framework based on a cluster mean-field approximation, which partially takes correlations into account, is developed to evaluate the stationary properties of the system. It is found that fundamental current-density relations in the system strongly depend on the strength and the sign of interactions, as well as on the range of interactions. For repulsive interactions stronger than some critical value, a mean-field theoretical approach predicts that increasing the range of interactions might lead to a change from unimodal to trimodal

^{*}Cade Spaulding and Hamid Teimouri contributed equally to the work.

^{**} Author to whom any correspondence should be addressed.

dependence in the flux-density fundamental diagram. However, it is not fully supported by extensive Monte Carlo computer simulations that test theoretical predictions. Although in most ranges of parameters a reasonable agreement between theoretical calculations and computer simulations is observed, there are situations when the cluster mean-field approach fails to describe properly the dynamics in the system. Theoretical arguments to explain these observations are presented. Our theoretical analysis clarifies the microscopic picture of how the range of interactions influences the dynamics of interacting molecular motors.

Keywords: asymmetric exclusion processes, molecular motors, long-range interactions

(Some figures may appear in colour only in the online journal)

1. Introduction

It is known that multiple intracellular processes are supported by special classes of active molecules known as motor proteins or biological molecular motors [1, 4, 7, 15]. Such processes include transport along cytoskeleton filaments, cell division, DNA replication and error correction, RNA transcription, synthesis of new protein molecules and many others [1, 4, 7, 14–16]. Molecular motors are frequently viewed as nanomachines that efficiently transform the chemical energy into mechanical work needed for their functioning. In recent years, a significant progress in understanding the microscopic mechanisms of individual motor proteins has been achieved from both experimental and theoretical points of view [7, 14–16, 31]. However, in cells the biological molecular motors typically work in groups, achieving high efficiency by coordinating their activities [15, 29]. At the same time, the molecular mechanisms of such cooperativity still remain not well understood [14, 23, 29, 30].

There are several experimental studies suggesting that some motor proteins might interact with each other during the transportation along the protein filaments [21, 26, 28, 32]. The conclusions from these investigations, however, are rather controversial. Some of them claimed that the interactions for kinesin motor proteins that move along microtubule filaments are weakly attractive [32], while others concluded that these interactions are stronger and more repulsive [28]. But the nature of such interactions and their ranges remain not well explained. There are also recent experimental measurements that clearly identified longer ranges of interactions and long-range cooperativity effects in kinesin motor proteins [21, 22]. All these observations support the importance of long-range interactions for transport of biological molecular motors.

Because most of the motor proteins typically move in a linear fashion, to understand their collective dynamics a powerful method of one-dimensional non-equilibrium multi-particle models, which are known as asymmetric simple exclusion processes, has been widely explored in theoretical studies [6, 11, 13, 17, 23, 24]. This approach has been extended to interacting molecular motors that lead to the development of the totally asymmetric exclusion process (TASEP) in which interactions are taken into account in a thermodynamically consistent fashion [5, 27]. It was later generalized to more realistic situations of biological transport [18–20]. Several other theoretical ideas to analyze the dynamics of interacting particles have been also proposed [2, 8–10, 12, 13, 24, 25, 33]. These developments allowed researchers to obtain several new unexpected results concerning the collective dynamics of interacting molecular motors. For example, it was argued that the particle flux through the system might increase for

weak repulsive forces in comparison with no interaction case. However, most current theoretical studies consider only short range interactions between the molecular motors, despite the fact that because of electrostatics and polar interactions (charged and polar groups on motor proteins) such interactions might have longer ranges. But one should also notice the theoretical treatment of longer interactions in reference [21].

In this paper, we present a theoretical investigation on the role of the range of interactions on dynamics of interacting molecular motors. More specifically, we considered a new TASEP model where not only nearest neighbors but also next-nearest-neighbors interactions are considered. Analysis of this model using a cluster mean-field approach that partially accounts for correlations in the system allows us to obtain a comprehensive theoretical predictions for the dynamic properties of the system. Theoretical analysis shows that extending the range of interactions brings a new physics into the system. It is predicted theoretically that a complex trimodal behavior is observed for fundamental current-density diagrams for strong repulsive interactions, while for attractions and weak repulsions a unimodal current-density relation is observed. This is a consequence of the longer range of interactions. We also estimated that the correlations between next-nearest neighbors are weaker and more short-range for repulsive interactions while for attractions they are stronger and more long-range. Theoretical predictions are probed with extensive Monte Carlo computer simulations, and it is found that the theoretical approach correctly describes the dynamics of the system for most ranges of parameters, however, the predictions of trimodality are not fully realized. The observed deviations are explained by larger local fluctuations in the particles densities that effectively decrease the correlations in the system for some sets of parameters. Thus, our analysis suggests that extending the range of interactions introduces qualitatively new phenomena in the complex process of the driven dynamics of interacting particles.

2. Theoretical analysis

2.1. Model

Let us consider a model in which transport of molecular motors along linear filaments is viewed as a unidirectional motion of multiple particles on a lattice with L ($L \gg 1$) sites, as shown in figure 1 (left). For simplicity, we consider a periodic boundary condition in which site L+1 is the same as the site 1, i.e., the particle dynamics on a ring will be analyzed. Each lattice site i ($1 \le i \le L$) is characterized by an occupation number τ_i . If the site i is occupied then $\tau_i = 1$, if it is empty then $\tau_i = 0$. Each lattice site can be covered by only one particle.

In addition to exclusion, the molecular motors in our model also interact via a long-range potential. Stimulated by the important role of electrostatics, we assume that this potential has the following dependence on the distance r between the particles $\phi(r) \simeq 1/r$. This means that two motors located m sites away from each will have the interaction energy E/m, where E is the energy of interaction for two nearest neighbors particles (in units of $k_B T$). It is important to note that E < 0 describes the repulsive interactions, while E > 0 corresponds to attractions. Previous theoretical studies considered only short-range interactions with m = 1. To the best of our knowledge, no interactions beyond the nearest neighbors have been considered so far. Our goal is to go beyond m = 1, and to clarify the role of the range of interactions on dynamics of interacting molecular motors. For convenience, we concentrate only on the situations that involve nearest neighbors (m = 1) and next nearest neighbors (m = 2), neglecting the interactions at longer distances ($m \ge 3$), although the analysis can be extended to longer ranges of interactions.

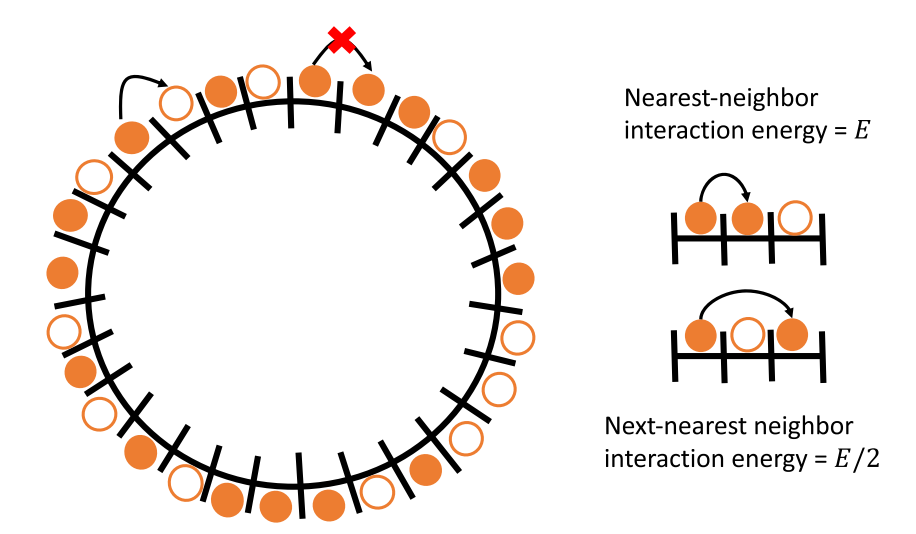


Figure 1. Schematic view of the TASEP model for particles with interactions on a ring of lattice sites (left). Particles move only in the clockwise direction. Filled symbols are particles and empty symbols are holes. Dependence of the interaction energy on the proximity of the neighboring motors (right). The interaction energy for nearest neighbor motors is E (in units of $k_B T$), while the interaction energy for the next-nearest neighbor configuration is E/2 (in units of $k_B T$). See text for more details on the model.

It is important to note here that interactions between real proteins in living systems are much more complex than what we assumed in our work. They involve van der Walls forces as well as electrostatic and polar interactions [3]. However, to understand the physics of extending the range of interactions, we chose a simplified long-range potential, which we hope still should help us to clarify some microscopic aspects of complex biological transport phenomena.

One should also connect parameters used in our theoretical analysis with real parameters that describe biological molecular motors. Since most motor proteins preferentially move in one direction, it is reasonable to utilize TASEP models. However, the absolute value of transition rates is not important because it only determines the time scale in our theoretical calculations and can be easily varied. More important quantity is energy of interactions. Since the absolute values of the interaction strength are not well known, we explored all possible ranges of interactions to obtain a full physical picture of the process.

The presence of potential modifies the dynamics of creating and breaking 'bonds' between the particles. We assume that two particles sitting next to each other form a kind of a 'stronger bond', while particles that are separated by one site form a kind of a 'weaker bond' due to interactions. The processes of creating and breaking these bonds can be viewed as opposing chemical transitions, which justifies the application of the detailed balance arguments [27]. More specifically, the ratio of forward and backward transition rates between two arbitrary states of the system, labeled i and j, can be written as

$$\frac{\text{Rate}(i \to j)}{\text{Rate}(j \to i)} = \exp\left[\frac{E_j - E_i}{k_{\text{B}}T}\right],\tag{1}$$

where E_i and E_j are total energies of interactions between all particles in the configurations i and j, respectively. This means that the ratio of the forward and the backward transition

rates between the states i and j is specified by the difference in energies of these states. It is important to note that in the system of interacting motor proteins, the detailed balance principle (equation (1)) can only be applied to characterize the local transitions between two individual motors that form or break bonds. However, the transitions between the collective configurations of the motor proteins are irreversible and thus do not follow the detailed balance.

To quantify these rates explicitly, we introduce two additional parameters,

$$q = \exp\left(\frac{E}{4k_{\rm B}T}\right), \qquad r = \exp\left(-\frac{E}{4k_{\rm B}T}\right).$$
 (2)

All possible transition rates can be expressed in terms of these two parameters, as we show explicitly below.

2.2. Cluster mean-field analysis

It has been argued before that because of interactions there are correlations between particles at neighboring sites in the TASEP model for interacting molecular motors [5, 19, 20, 27]. These correlations are much stronger in comparison with the system without interactions. Neglecting such correlations leads to unphysical behavior for strong interactions between the molecular motors [27]. This indicates that any successful theoretical analysis must take into account these correlations. This is the main reason for us to utilize a theoretical method that is based on *cluster mean-field* calculations.

In this approach, the dynamics inside of the cluster of several lattice sites is considered exactly, while the correlations between different clusters are neglected. Since in our model the interactions do not extend beyond the two lattice sites from the given particle, it seems reasonable to explore a minimal three-site mean-field cluster analysis. To understand the dynamics in the system, we consider a sequence of six lattice sites, as presented in figure 2, where we follow the transitions of the particle from the 3rd site to the 4th site. Because the lattice ring is homogeneous, this procedure will allow us to evaluate the dynamics at any site of the ring. The stationary probability of a configuration with six sequential sites $(\tau_{i-2}, \tau_{i-1}, \tau_i, \tau_{i+1}, \tau_{i+2}, \tau_{i+3})$ is given by $P(\tau_{i-2}, \tau_{i-1}, \tau_i, \tau_{i+1}, \tau_{i+2}, \tau_{i+3})$. The cluster mean-field approach postulates that the probability of such six-site clusters can be presented as a normalized product of three-site cluster probabilities [19, 20]

$$P(\tau_{i-2}, \tau_{i-1}, \tau_i, \tau_{i+1}, \tau_{i+2}, \tau_{i+3}) = \frac{P(\tau_{i-2}, \tau_{i-1}, \tau_i) P(\tau_{i-1}, \tau_i, \tau_{i+1}) P(\tau_i, \tau_{i+1}, \tau_{i+2}) P(\tau_{i+1}, \tau_{i+2}, \tau_{i+3})}{P(\tau_{i-1}, \tau_i) P(\tau_i, \tau_{i+1}) P(\tau_{i+1}, \tau_{i+2})}.$$
(3)

Note that the denominator accounts for the fact that in the product of three-site cluster probabilities some sites are accounted twice. The physical meaning of this expression is that the probability to have a given large configuration of sites is equal to the normalized product of probabilities of shorter clusters of sites.

For the six-site cluster there are 16 different transitions as illustrated in figure 2. This is because we always start in the configuration with the particle in the 3rd site and empty 4th site. Other four sites in the cluster can be in one of two states (occupied or empty), giving the total number of distinguishable configurations to be equal to $2^4 = 16$. Each transition is associated with the energy change and the corresponding transition rates can be found from the detailed balance arguments [see equation (1)]. For example, transitions 1, 8, 9, 11, 12 and 16 in figure 2 are not associated with any energy changes, and we define the corresponding transition rates to be equal to one. Now let us consider transitions 2 and 6 in figure 2. They can be viewed as

	Transition	Transition Rate	Energy Change
1	\bigcirc	1	0
2	$ \bigcirc \bigcirc \longrightarrow \bigcirc \bigcirc \bigcirc$	r	-E/2
3	$\bigcirc \bullet \bullet \rightarrow \bigcirc \bigcirc \bigcirc$	r	-E/2
4		r^2	— Е
5	\bigcirc	q	E/2
6	\bigcirc	q	E/2
7	\bigcirc	q^2	Ε
8	$\bigcirc\bigcirc\bigcirc\rightarrow\bigcirc\bigcirc\bigcirc\bigcirc$	1	0
9	$\bigcirc\bigcirc\bigcirc\bigcirc\rightarrow\bigcirc\bigcirc\bigcirc\bigcirc$	1	0
10	$\bigcirc\bigcirc\bigcirc\rightarrow\bigcirc\bigcirc\bigcirc\bigcirc\bigcirc$	q	E/2
11	$\bigcirc \hspace{0.1cm} \bullet \hspace{0.1cm} \bullet \hspace{0.1cm} \bigcirc \hspace{0.1cm} \longrightarrow 0.1cm$	1	0
12	$\bigcirc \bullet \bullet \rightarrow \bigcirc \bigcirc \bullet$	1	0
13	$\bigcirc \hspace{0.1cm} \bullet \hspace{0.1cm} \bullet \hspace{0.1cm} - \hspace{0.1cm} \bigcirc \hspace{0.1cm} \bullet \hspace{0.1cm} \hspace{0.1cm} \hspace{0.1cm} \bullet \hspace{0.1cm} \hspace{0.1cm} \hspace{0.1cm} \bullet \hspace{0.1cm} \hspace{0.1cm} \bullet \hspace{0.1cm} 0.$	q	E/2
14		r	-E/2
15	$ \bigcirc \bigcirc$	r	-E/2
16		1	0

Figure 2. A list of all possible particle transitions, corresponding energy changes and transition rates for a six-site cluster of the lattice. Only the transition of the particle at the third site to the empty fourth is considered.

opposing to each other because in the transition 6 the weak bond is created, while the same weak bond is broken in the transition 2. The energy change associated with this process is just E/2. Then the transition rate for the process 2 is set to be equal to r, while for the process 6 it is set to be equal to q. This satisfies the detailed balance arguments because $q/r = \exp(E/2)$. Similar arguments can be applied to all allowed transitions, providing the explicit expressions for different transition rates as shown in figure 2.

The overall particle flux in the system will have 16 terms to reflect the different transitions from 16 configurations (see figure 2), and it has the following form,

$$J = P_{001000} + qP_{001001} + qP_{001010} + q^2P_{001011} + rP_{011000} + P_{011001} + P_{011010} + qP_{011011} + rP_{101000} + P_{101001} + P_{101010} + qP_{101011} + r^2P_{111000} + rP_{111001} + rP_{111010} + P_{111011}.$$

$$(4)$$

Each probability of the six-site cluster can be expressed via three-site probabilities using equation (3). There are eight such probabilities labeled as P_{111} , P_{110} , P_{100} , P_{010} , P_{011} , P_{001} , P_{101} and P_{000} . Due to the conservation of probability, they are related via a normalization condition,

$$P_{111} + P_{110} + P_{100} + P_{010} + P_{011} + P_{001} + P_{101} + P_{000} = 1. (5)$$

Let us also simplify the notations by defining

$$P_{111} = a;$$
 $P_{100} = b;$ $P_{101} = c;$ $P_{100} = d;$ $P_{011} = e;$ $P_{010} = f;$ $P_{001} = g;$ $P_{000} = h.$ (6)

One could also notice that two-site cluster probabilities can be also expressed via three-site probabilities,

$$P_{11} = a + b = a + e;$$
 $P_{00} = g + h = d + h;$ $P_{01} = P_{10} = c + d = b + f.$ (7)

Now, we can obtain an explicit expression for the particle current in the system in terms of the three-site cluster probabilities,

$$J = \frac{abcfr}{(a+b)(c+d)^2} + \frac{bcfe}{(a+b)(c+d)^2} + \frac{abdhr^2}{(a+b)(c+d)(g+h)}$$

$$+ \frac{bdhre}{(a+b)(c+d)(g+h)} + \frac{abdgr}{(a+b)(c+d)(g+h)} + \frac{bdge}{(a+b)(c+d)(g+h)}$$

$$+ \frac{bcqe^2}{(a+b)(c+d)^2} + \frac{abce}{(a+b)(c+d)^2} + \frac{c^2f^2}{(c+d)^3} + \frac{c^2fqe}{(c+d)^3}$$

$$+ \frac{cf^2gq}{(c+d)^3} + \frac{dfg^2q}{(c+d)^2(g+h)} + \frac{cdfhr}{(c+d)^2(g+h)} + \frac{cdfg}{(c+d)^2(g+h)}$$

$$+ \frac{dfgh}{(c+d)^2(g+h)} + \frac{cfgq^2e}{(c+d)^3}.$$
(8)

This means that the dynamics in the system of interacting molecular motors can be fully described if we determine all three-site cluster probabilities.

Thus, we need to explicitly find 8 unknown variables, (a, b, c, d, e, f, g, h). To do so, eight independent equations are required. To find some of these equations, we notice that the system presented in figure 1 (left) has a particle–hole symmetry: the clockwise motion of the particles is identical to the counterclockwise motion of the holes. Now, using these symmetry arguments and the normalization, one can easily derive five equations:

$$g = d;$$
 $e = b;$
 $f = c + d - b;$ $c = -a - d - b + \rho;$
 $h = 1 - a - b - c - d - e - f - g.$ (9)

where ρ is the bulk density (or the probability to find the particle at a given site). Three more equations are needed, and they can be derived from the corresponding master equations for probabilities P_{111} , P_{110} , and P_{000} ,

$$\frac{\mathrm{d}P_{111}}{\mathrm{d}t} = q^2 P_{001011} + q P_{011011} + q P_{101011} - r^2 P_{111000} - r P_{111001} - r P_{111010};\tag{10}$$

$$\frac{\mathrm{d}P_{110}}{\mathrm{d}t} = -rP_{011000} - P_{011001} + qP_{011010} - qP_{011011} + P_{101010} + rP_{111010};\tag{11}$$

$$\frac{\mathrm{d}P_{000}}{\mathrm{d}t} = qP_{001001} + qP_{001010} + q^2P_{001011} - rP_{011000} - rP_{101000} - r^2P_{111000}. \tag{12}$$

We are interested in the stationary dynamics when the left sides of these equations will be zero, and combining equations (10)–(12) with equation (9) yields a system of three non-linear equations for variables a, b and d,

$$0 = \frac{b^{3}q(-a-b-d+\rho)}{(a+b)(-a-b+\rho)^{2}} - \frac{abd^{2}r}{(a+b)(a+b-2\rho+1)(-a-b+\rho)} + \frac{bdq^{2}(-a-2b+\rho)(-a-b-d+\rho)}{(-a-b+\rho)^{3}} + \frac{bq(-a-2b+\rho)(-a-b-d+\rho)^{2}}{(-a-b+\rho)^{3}} + \frac{bq(-a-2b+\rho)(-a-b-d+\rho)^{2}}{(a+b)(a+b-2\rho+1)(-a-b+\rho)} + \frac{abdr^{2}(a+b-d-2\rho+1)}{(a+b)(a+b-2\rho+1)(-a-b+\rho)} + \frac{a^{3}q(-a-2b+\rho)}{(a+b-2\rho+1)(-a-b+\rho)^{2}} + \frac{b^{2}q(-a-2b+\rho)(-a-b-d+\rho)}{(-a-b+\rho)^{3}} + \frac{dq(-a-2b+\rho)^{2}(-a-b-d+\rho)}{(-a-b+\rho)^{3}} + \frac{dq(-a-2b+\rho)^{2}(-a-b-d+\rho)}{(a+b)(a+b-2\rho+1)(-a-b+\rho)} + \frac{a^{3}q(-a-2b+\rho)}{(a+b-2\rho+1)(-a-b+\rho)^{2}} + \frac{b^{2}q(-a-2b+\rho)(-a-b-d+\rho)}{(a+b)(a+b-2\rho+1)(-a-b+\rho)} + \frac{b^{2}q(-a-2b+\rho)(-a-b-d+\rho)}{(a+b)(-a-b+\rho)^{2}} + \frac{b^{2}q(-a-2b+\rho)(-a-b-d+\rho)}{(a+b)(-a-b+\rho)^{2}} + \frac{b^{2}q(-a-2b+\rho)(-a-b-d+\rho)}{(a+b)(-a-b+\rho)^{2}} + \frac{b^{2}q(-a-2b+\rho)(-a-b-d+\rho)}{(a+b)(-a-b+\rho)^{2}} + \frac{abr(-a-2b+\rho)(-a-b-d+\rho)}{(a+b)(-a-b+\rho)^{2}} + \frac{(-a-2b+\rho)^{2}(-a-b-d+\rho)^{2}}{(-a-b+\rho)^{3}} + \frac{abr(-a-2b+\rho)(-a-b-d+\rho)}{(a+b)(-a-b+\rho)^{2}} .$$
(15)

We note that these equations have only two input parameters: the interaction energy E and the particle density ρ . For any arbitrary value of E and ρ , equations (9) and (13)–(15) can be solved numerically exactly, providing the explicit expressions for the three-site cluster probabilities and allowing us to obtain a comprehensive description of the dynamics in the system of interacting molecular motors with extended range of interactions at all possible interactions

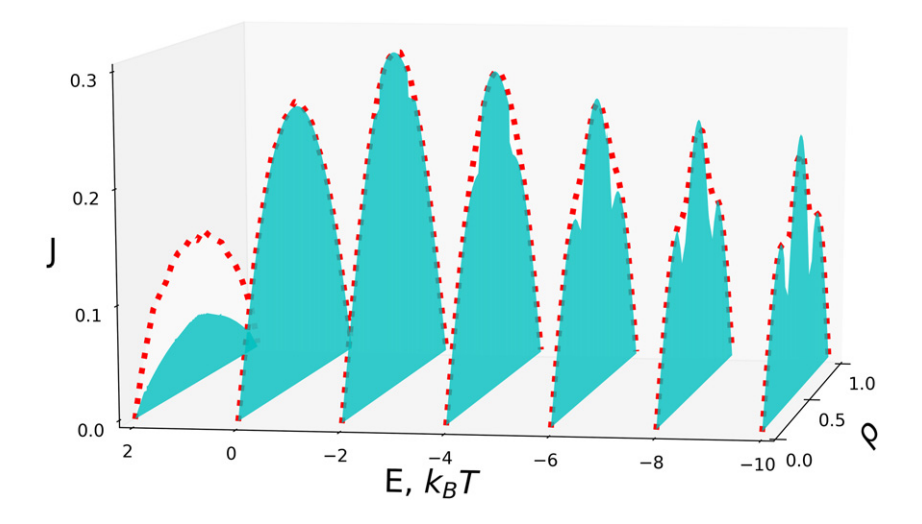


Figure 3. The particle flux in the system of interacting molecular motors for different interactions and densities. Lines are theoretical predictions. Symbols are from Monte Carlo computer simulations. In computer simulations, L = 500 was utilized.

and particle densities. In this process, since multiple solutions of non-linear equations are possible, we choose physically meaningful solutions with densities lying between zero and one. The results are presented in figure 3 where they are also compared with Monte Carlo computer simulations. One can see that our theoretical model agrees quite well with simulations for repulsions, except for few small intervals, and we explain below the reason for these deviations. The agreement is also only qualitative for attractive interactions, but this has been already observed for the systems with only nearest-neighbor interactions [20]. This is a consequences of longer correlations for attractive potentials.

For Monte Carlo computer simulations, we chose a lattice size of L=500. As we checked, increasing the size of the lattice did not change the results. A random sequential update was used for all simulations. The particle flux was averaged over 20 000 Monte Carlo steps and the first 20% of them were removed to ensure that the system reaches the stationary state.

2.3. Analytical results for limiting situations

Although our theoretical approach can evaluate the dynamics in the system of interacting molecular motors with extended range of interactions numerically exactly, there are several limiting cases when a full analytical description can be obtained. This allows us to test the validity of our theoretical method as well as to understand better the microscopic picture of these complex processes.

2.3.1. Strongly-attracting particles $(E \to +\infty)$. In this case, we have $q \to \infty$ and $r \to 0$, which leads to only two non-zero three-site cluster probabilities, $P_{111} = a = \rho$ and $P_{000} = h = 1 - \rho$. Physically it means that all particles on the ring will be jammed in one large continuous cluster that will not allow for any particle flux, J = 0. This is an expected behavior because for the particle to break out from the large cluster will cost an infinite amount of energy, and for this reason this does not happen.

2.3.2. Non-interacting particles (E = 0). In this limit, we have q = r = 1, and it can be shown that three-site cluster probabilities are given by the following expressions:

$$P_{111} = \rho^3;$$
 $P_{110} = P_{101} = P_{011} = \rho^2 (1 - \rho);$
 $P_{100} = P_{010} = P_{001} = \rho (1 - \rho)^2;$ $P_{000} = (1 - \rho)^3.$ (16)

Substituting these results into equation (8), we obtain the particle flux as $J = \rho(1 - \rho)$.

These results can be easily interpreted. Without interactions, there is no correlations in the particle occupancy, and the three-site cluster probabilities can be easily obtained as a product of three one-site probabilities with the occupied site probability equal to ρ and the empty site probability equal to $1-\rho$. These are well-known results for the TASEP model without interactions [6].

2.3.3. Strongly-repulsive particles $(E \to -\infty)$. In this case, we have $q \to 0$ and $r \to \infty$, which significantly simplifies the analysis. In addition, it is convenient to perform the calculations for three different ranges of particle densities.

For the first low-density region, when $0 \le \rho \le 1/3$, one cannot have two particles next to each other due to strong repulsion. Because the density is not high, this can be accomplished, and it leads to

$$P_{111} = P_{110} = P_{101} = P_{011} = 0;$$

 $P_{100} = P_{010} = P_{001} = \rho;$ $P_{000} = 1 - 3\rho;$ (17)

and the following results for the two-site cluster probabilities,

$$P_{10} = \rho;$$
 $P_{11} = 0;$ $P_{00} = 1 - 2\rho.$ (18)

In the limit of strong repulsions, the only contribution to the flux is due to one configuration 001 000 out of 16 possible six-site configurations. Thus, the particle flux is given by,

$$J = P_{001000} = \frac{P_{001}P_{010}P_{100}P_{P_{000}}}{P_{01}P_{01}P_{00}} = \frac{\rho(1-3\rho)}{1-2\rho},\tag{19}$$

which also corresponds to the flux of non-interacting trimers [18]. Therefore, for $0 \le \rho \le 1/3$, for strong repulsions the interacting molecular motors with the increased range of interactions behave like non-interacting timers. This is clearly a result of the increased range that does not allow other particles to come to the given particle closer than two sites apart, which effectively mimicks the dynamics of non-interacting trimers.

For intermediate densities, $1/3 \le \rho \le 2/3$, it is not possible to avoid the contact of two particles, but the situation with three particles together cannot happen due to the strong repulsions. In this case, we have

$$P_{111} = P_{000} = 0;$$
 $P_{110} = P_{101} = P_{011} = \rho - 1/3;$ $P_{100} = P_{001} = P_{010} = 2/3 - \rho.$ (20)

There are four six-site configurations that can produce the particle flux, 101 010, 101 001, 011 010 and 011 001. This leads to the following expression for flux,

$$J = P_{101010} + P_{101001} + P_{011010} + P_{011001} = 3\rho(3\rho - 1)(2 - 3\rho)(1 - \rho).$$
 (21)

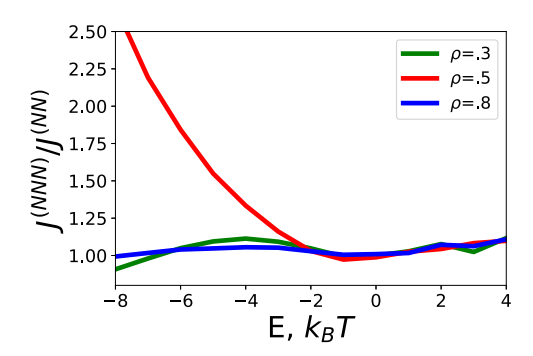


Figure 4. Predictions of Monte-Carlo computer simulations for the ratio of particle fluxes for TASEP with next-nearest neighbor interactions $J^{(NNN)}$ (extended rage) and TASEP with nearest-neighbor interactions $J^{(NN)}$ (short range). In simulations, L=500 was utilized.

Note that these theoretical arguments predict that the current will disappear for $\rho = 1/3$ and $\rho = 2/3$ in the limit of strong repulsions. Moreover, similar expression for the particle flux was obtained for only having nearest-neighbors interactions [18]:

$$J^{(NN)} = \frac{\rho(1-2\rho)}{(1-\rho)}.$$
 (22)

One can see that for $\rho = \frac{1}{2}$ the flux $J^{(NN)}$ is approaching zero, and this allows us to understand better the results in figure 4.

Finally, for the highest density region, $2/3 \le \rho \le 1$, the results can be obtained easily using a particle-hole symmetry from the first low-density region calculations. For this purpose, we need to change $0 \leftrightarrow 1$ and $\rho \leftrightarrow (1-\rho)$. Then we obtain for the three-site probabilities,

$$P_{100} = P_{010} = P_{001} = P_{000} = 0;$$

 $P_{111} = 3\rho - 2;$ $P_{110} = P_{101} = P_{100} = 1 - \rho;$ (23)

and the following results for the two-site probabilities,

$$P_{10} = 1 - \rho;$$
 $P_{11} = 2\rho - 1;$ $P_{00} = 0.$ (24)

In this case, the only surviving term in particle flux is P_{111011} . Thus

$$J = P_{111011} = \frac{(1-\rho)(3\rho - 2)}{2\rho - 1}. (25)$$

This corresponds to the flux of non-interacting trimers of holes.

Thus, the combined expressions for the particle flux in the strong repulsion limit for interacting molecular motors with extended range of interactions is given by,

$$J \simeq \begin{cases} \frac{\rho(1-3\rho)}{1-2\rho}; & 0 \leqslant \rho \leqslant 1/3; \\ 3\rho(3\rho-1)(2-3\rho)(1-\rho); & 1/3 \leqslant \rho \leqslant 2/3; \\ \frac{(1-\rho)(3\rho-2)}{2\rho-1}; & 2/3 \leqslant \rho \leqslant 1. \end{cases}$$
 (26)

One can see that this function is continuous at $\rho = \frac{1}{3}$ and $\rho = \frac{2}{3}$, as expected.

2.4. Fundamental current-density diagrams

Our theoretical method allows us to explicitly evaluate the relations between the particle currents and densities for all possible inter-molecular interactions, as shown in figure 3. It also provides an important insights on the role of the extended range of interactions. A unimodal current-density fundamental diagram is observed for attractions and for weak repulsion with the largest current to be achieved at $\rho=1/2$. Increasing the strength of repulsion from the no-interactions case E=0 first leads to the increase in the maximal current (at $\rho=1/2$) at $E\simeq -2$. But the further increase in the repulsion strength leads to the lowering of the maximal current. The interesting behavior starts for repulsions stronger that $E\simeq -6$: the originally unimodal curve with one maximum transforms into the trimodal curve that exhibits three maxima and two minima. The minimum currents are predicted for $\rho=1/3$ and $\rho=2/3$. As the repulsion increases, our theory predicts that the currents at these special locations will eventually reach zero, in agreement with our arguments that the system of interacting molecular motors with the extended range of parameters for $E\to -\infty$ behaves like a system of non-interacting trimers.

We tested the predictions of the three-site cluster mean-field theory with Monte Carlo computer simulations. Excellent agreement is found for all densities for attractive and weakly repulsive interactions: see figure 3. However, there are some deviations from theoretical calculations for strong repulsions near the regions where the minimal current is predicted (around $\rho=1/3$ and $\rho=2/3$). Instead of minimal current at these regions, simulations suggest that the particle current becomes almost constant and independent of density, connecting the increasing branches of the current–density curves. This observation will be explained below.

One of the surprising results of the TASEP model with interactions is the observation of the increase in the maximal particle current for weak repulsions [5, 27]. But it was found for the system with short-range interactions. Using our theoretical approach, we can probe how the extended range of interactions will affect this result. In figure 4, we present the ratio of the particle currents for the system with the extended range (NNN) over the particle current for the system with the short-range (NN) for different particle densities. For low densities ($\rho = 0.3$) and for high densities ($\rho = 0.8$) there is not much effect on the increasing the flux by extending the range of interactions. However, the strong effect is observed for the maximal current for $\rho = 1/2$. In this case, the flux increases more for the system with extended range of interactions, and the effect is larger for stronger repulsions. One can explain this by noting that for low densities particles can be found at the distances where the interactions do not affect them, while for high densities the particle transitions in most cases are not associated with energy changes. Only for $\rho = 1/2$ the effect of interactions is maximal and the extended range helps to make it even stronger.

3. Correlation functions

To understand better the microscopic mechanisms of the processes that are taking place during the transport of interacting molecular motors, it is important to analyze the correlations functions that measure the degree of correlations in the system. One could define the nearest-neighbor correlation function,

$$C^{(\mathrm{NN})} = \langle n_i, n_{i+1} \rangle - \langle n_i \rangle \langle n_{i+1} \rangle = P_{11} - \rho^2, \tag{27}$$

which can be easily calculated using our theoretical approach. However, due to the extended range of interactions in our system, this correlation function might not properly capture the relevant processes in the system. Alternatively, we introduce the next-nearest neighbor correlation

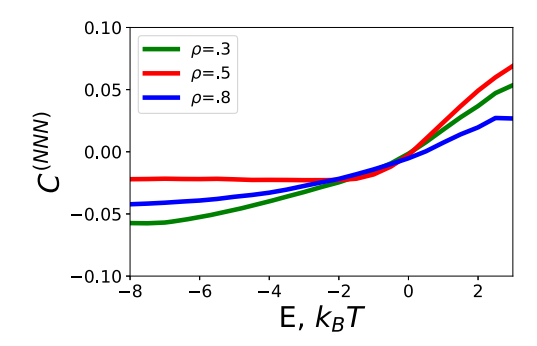


Figure 5. Results of Monte-Carlo simulations for the next-nearest neighbor correlation function $C^{(\mathrm{NNN})}$ as a function of the interaction energy (*E*). In simulations, L=500 was utilized.

function $C^{(NNN)}$,

$$C^{(\text{NNN})} = \langle n_i, n_{i+2} \rangle - \langle n_i \rangle \langle n_{i+2} \rangle, \qquad (28)$$

where the corresponding two-point function $\langle n_i, n_{i+2} \rangle$ is defined as

$$\langle n_i, n_{i+2} \rangle = \sum_{n_i} \sum_{n_i+1} \sum_{n_i+2} n_i n_{i+2} P(n_i, n_{i+1}, n_{i+2}) = P_{101} + P_{111},$$
 (29)

and $\langle n_i \rangle = \langle n_{i+2} \rangle = \rho$. Thus, $C^{(\text{NNN})}$ is given by

$$C^{(\text{NNN})} = P_{101} + P_{111} - \rho^2. \tag{30}$$

One can see that the main difference between the nearest-neighbor correlation function and the next-nearest neighbor correlation function is that $C^{(NNN)}$ is expressed in terms of three-site clusters probabilities while $C^{(NN)}$ includes only the two-site clusters probabilities.

Figure 5 presents the next-nearest neighbor correlation functions, as estimated from the Monte Carlo simulations, as a function of the interactions for different particle densities. One can see that for attractive interactions these correlations are positive, while for repulsions they are negative. These results can be easily explained. For E>0 it is more probable to find another particle at the nearest-neighbor site due to attractive interactions, and this leads to positive correlations. Similarly, for E<0 it is less probable to find the particle at the nearest-neighbor site due to repulsion, and this leads to the negative correlations. It is important to note that these correlations are due to the extended range of interactions and they are essentially absent in the system with short-range interactions.

One might illustrate better the effect of the range of interactions by considering several limiting case where these correlation functions can be estimated fully analytically. For the case of no interactions (E=0), it was already shown that $P_{111}=\rho^3$ and $P_{111}=\rho^2(1-\rho)$. Substituting these results into equation (30) produces $C^{(NNN)}=0$, i.e., there are no nextnearest neighbor interactions, as expected. Analytical results can be also obtained in the limit

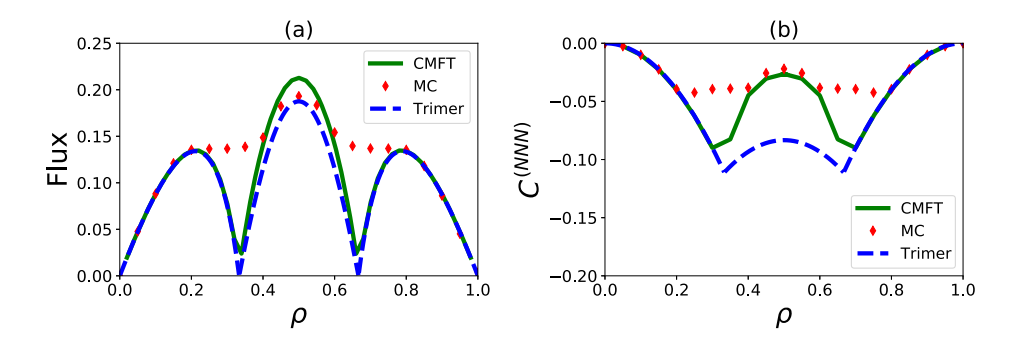


Figure 6. Predictions of Monte-Carlo computer simulations and cluster mean-field theory for $E = -20k_{\rm B}T$ for interacting molecular motors and for non-interacting trimers. (a) The particle flux (J) as a function of particle density (ρ); and (b) the next-nearest neighbor correlation function ($C^{({\rm NNN})}$) versus particle density.

of strong repulsions, $E \to -\infty$. Using equation (17), we derive

$$C^{(\text{NNN})} \simeq \begin{cases} -\rho^2; & 0 \leqslant \rho \leqslant 1/3\\ \rho - \frac{1}{3} - \rho^2; & 1/3 \leqslant \rho \leqslant 2/3\\ 2\rho - 1 - \rho^2; & 2/3 \leqslant \rho \leqslant 1. \end{cases}$$
(31)

Our theoretical three-site cluster mean-field approach is successful in describing the dynamics of interacting molecular motors with the extended range of interactions for attractions and weak repulsions. Only for strong repulsions, theory agrees with simulations quantitatively for $\rho < 0.2$, $\rho > 0.8$ and semi-quantitatively for $0.4 < \rho < 0.6$, while the deviations between computer simulations and theoretical predictions are found near the regions of $\rho \simeq 1/3$ and $\rho \simeq 2/3$. In these cases, theory predicts a minimal particle current which is not observed in Monte Carlo simulations at all. Importantly, the trimodal phase diagram predicted by the mean-field method is not supported by computer simulations. To understand the origin of such deviations, we plot in figure 6 the particle flux and the next-nearest neighbor correlation function for very strong repulsion (E = -20). The Monte Carlo computer simulations are compared with the calculations of the three-site cluster mean-field approach for interacting particles with the extended range and for non-interacting trimers [19]. This is because for such strong repulsions one could expect that the dynamics of non-interacting trimers might provide a good description, as we argued above.

Note that our calculations of the 'trimers' theory are done in the following way. For small densities ($\rho < 1/3$) it is assumed that the trimer corresponds to 111 clusters, for intermediate densities ($1/3 < \rho < 2/3$) the trimer describes 110 clusters, while for high densities ($2/3 < \rho < 1$) the trimer corresponds to 100 clusters. We calculate the fluxes of such particles in all different regimes. Of course, in real system particles follow slightly different dynamics since the monomer transitions are taking place. However, the trimer approach might be a very reasonable description for very strong repulsions.

Comparison of figures 6(a) and (b) suggests that the theoretical calculations do not work well in the region of minimal currents due to overestimating the negative correlation in the system. In reality, the negative next-nearest neighbor interactions are not as strong. The possible reason for such observations is the following. Let us consider for simplicity the case $\rho = 1/3$. The particle density in the system constantly fluctuates. This means that there are segments

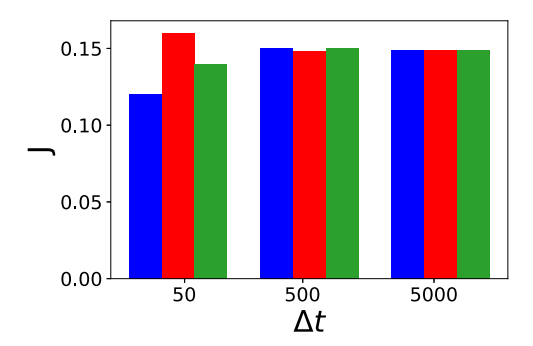


Figure 7. Particle fluxes (J_1, J_2, J_3) at three different positions along the lattice versus the averaging time windows Δt . The following parameters have been used for calculations: $\rho = 1/3$, E = -10 and the size of the system is L = 500.

where the density is larger than 1/3 and there are segments where the density is smaller than 1/3. But for such densities, high currents will be realized (see branches in the fundamental diagram in figure 6(a)). As the result, the fluctuations will wash out the negative correlations and larger particle fluxes are observed. This is because the densities slightly larger or slightly smaller than $\rho = 1/3$ support larger particle currents. The cluster mean-field theory does not account for such fluctuations, and this is the reason for differences between theoretical calculations and computer simulations. Note that when the theory correctly captures the correlations (e.g., near $\rho = 1/2$) the agreement between the simulations and theoretical predictions is much better.

To support our arguments that density fluctuations lead to observed particle currents, in figure 7 we presented histograms of particle fluxes simultaneously measured at three different locations of the system (far away from each other) as a function of the averaging time windows. One can see that even for very short time windows zero fluxes, which are predicted by the mean-field theory, are not observed, and for longer times the averaging is taking place, as expected. These results show that there are significant density fluctuations in the system that are not captured by the cluster mean-field approach.

Our theoretical calculations show the importance of the range of interactions for understanding the dynamics of molecular motors. Varying the range can strongly effect the molecular fluxes. This also suggests that together with the strength of interactions and other parameters it might be used to efficiently regulate the transport of motor proteins.

4. Summary and conclusions

We presented a theoretical study on the role of the extended range of interactions in dynamics of interacting molecular motors. Our analysis is based on investigating the TASEP model of particles with nearest and next-nearest interactions that move unidirectionally along the lattice of sites. To account for correlations in the system that are driven by interactions we developed a cluster mean-field theory that allowed to evaluate numerically exactly the dynamic properties in the system in the large range of parameters. Theoretical calculations are also supplemented by extensive Monte Carlo computer simulations. It is found from theoretical calculations that a unimodal fundamental current—density diagrams will be observed for attractive and weak repulsions. For stronger than some critical value of the repulsion, it is predicted that the flux-density relation will exhibit a trimodal shape. This is the result of the extended

range of interactions. Computer simulations agree with theoretical predictions for most situations except for the regions near the minimal current for strong repulsions. It is argued that the differences between the theoretical predictions and computer simulations are due to fluctuations that lower the amplitude of correlations at these regions. Our theoretical analysis shows how the extended range of interactions influences the topology of fundamental diagrams, the correlations and the particle currents, clarifying important microscopic features of complex non-equilibrium dynamic processes.

While our theoretical approach considered only the situation when interactions affect only nearest and next-nearest particles, it can be extended for longer ranges of interactions. Based on our analysis presented in this work, we expect that longer ranges of interactions will affect the dynamics only at repulsions. It will lead to the increased maximal current, increased correlations and more complex fundamental diagrams that might exhibit multi-modal shapes that probably will be washed out by fluctuations in the system. It will be interesting to test these predictions in more quantitative theoretical models and more advanced computer simulations.

Acknowledgments

The work was supported by the Welch Foundation (C-1559), by the NSF (CHE-1953453 and MCB-1941106), and by the Center for Theoretical Biological Physics sponsored by the NSF (PHY-2019745).

Data availability statement

All data that support the findings of this study are included within the article (and any supplementary files).

ORCID iDs

Hamid Teimouri https://orcid.org/0000-0002-3319-1187
Anatoly B Kolomeisky https://orcid.org/0000-0001-5677-6690

References

- [1] Alberts B, Johnson A, Lewis J, Raff M, Roberts K and Walter P 2007 *Molecular Biology of the Cell* (New York: Garland Science)
- [2] Antal T and Schütz G M 2000 Asymmetric exclusion process with next-nearest-neighbor interaction: some comments on traffic flow and a nonequilibrium reentrance transition *Phys. Rev.* E 62 83
- [3] Boström M, Williams D R M and Ninham B W 2001 Specific ion effects: why DLVO theory fails for biology and colloid systems *Phys. Rev. Lett.* 87 168103
- [4] Bressloff P C and Newby J M 2013 Stochastic models of intracellular transport Rev. Mod. Phys. 85 135
- [5] Celis-Garza D, Teimouri H and Kolomeisky A B 2015 Correlations and symmetry of interactions influence collective dynamics of molecular motors J. Stat. Mech. P04013
- [6] Chou T, Mallick K and Zia R K P 2011 Non-equilibrium statistical mechanics: from a paradigmatic model to biological transport Rep. Prog. Phys. 74 116601
- [7] Chowdhury D 2013 Stochastic mechano-chemical kinetics of molecular motors: a multidisciplinary enterprise from a physicist's perspective *Phys. Rep.* 529 1–197

- [8] Dierl M, Einax M and Maass P 2013 One-dimensional transport of interacting particles: currents, density profiles, phase diagrams, and symmetries *Phys. Rev.* E 87 062126
- [9] Dierl M, Maass P and Einax M 2011 Time-dependent density functional theory for driven lattice gas systems with interactions *Europhys. Lett.* 93 50003
- [10] Dierl M, Maass P and Einax M 2012 Classical driven transport in open systems with particle interactions and general couplings to reservoirs *Phys. Rev. Lett.* 108 060603
- [11] Dong J, Klumpp S and Zia R K P 2012 Entrainment and unit velocity: surprises in an accelerated exclusion process *Phys. Rev. Lett.* 109 130602
- [12] Hager J S, Krug J, Popkov V and Schütz G M 2001 Minimal current phase and universal boundary layers in driven diffusive systems *Phys. Rev.* E 63 056110
- [13] Klumpp S and Lipowsky R 2004 Phase transitions in systems with two species of molecular motors Europhys. Lett. 66 90
- [14] Kolomeisky A B 2013 Motor proteins and molecular motors: how to operate machines at the nanoscale J. Phys.: Condens. Matter 25 463101
- [15] Kolomeisky A B 2015 Motor Proteins and Molecular Motors (Boca Raton, FL: CRC Press)
- [16] Kolomeisky A B and Fisher M E 2007 Molecular motors: a theorist's perspective Annu. Rev. Phys. Chem. 58 675–95
- [17] Lipowsky R, Klumpp S and Nieuwenhuizen T M 2001 Random walks of cytoskeletal motors in open and closed compartments Phys. Rev. Lett. 87 108101
- [18] Midha T, Gomes L V F, Kolomeisky A B and Gupta A K 2018 Theoretical investigations of asymmetric simple exclusion processes for interacting oligomers J. Stat. Mech. 053209
- [19] Midha T, Kolomeisky A B and Gupta A K 2018 Effect of interactions for one-dimensional asymmetric exclusion processes under periodic and bath-adapted coupling environment J. Stat. Mech. 043205
- [20] Midha T, Kolomeisky A B and Gupta A K 2018 Interactions in nonconserving driven diffusive systems Phys. Rev. E 98 042119
- [21] Miedema D M, Kushwaha V S, Denisov D V, Acar S, Bernard N, Peterman E J G and Schall P 2017 Correlation imaging reveals specific crowding dynamics of kinesin motor proteins *Phys. Rev.* X 7 041037
- [22] Muto E, Sakai H and Kaseda K 2005 Long-range cooperative binding of kinesin to a microtubule in the presence of ATP J. Cell Biol. 168 691–6
- [23] Neri I, Kern N and Parmeggiani A 2013 Exclusion processes on networks as models for cytoskeletal transport New J. Phys. 15 085005
- [24] Pinkoviezky I and Gov N S 2013 Modelling interacting molecular motors with an internal degree of freedom New J. Phys. 15 025009
- [25] Popkov V and Schütz G M 1999 Steady-state selection in driven diffusive systems with open boundaries Europhys. Lett. 48 257
- [26] H Roos W, Campàs O, Montel F, Woehlke G, Spatz J P, Bassereau P and Cappello G 2008 Dynamic kinesin-1 clustering on microtubules due to mutually attractive interactions *Phys. Biol.* 5 046004
- [27] Teimouri H, Kolomeisky A B and Mehrabiani K 2015 Theoretical analysis of dynamic processes for interacting molecular motors J. Phys. A: Math. Theor. 48 065001
- [28] Telley I A, Bieling P and Surrey T 2009 Obstacles on the microtubule reduce the processivity of kinesin-1 in a minimal in vitro system and in cell extract Biophys. J. 96 3341–53
- [29] McLaughlin R T, Diehl M R and Kolomeisky A B 2016 Collective dynamics of processive cytoskeletal motors Soft Matter 12 14–21
- [30] Uppulury K, Efremov A K, Driver J W, Jamison D K, Diehl M R and Kolomeisky A B 2012 How the interplay between mechanical and nonmechanical interactions affects multiple kinesin dynamics *J. Phys. Chem.* B 116 8846–55
- [31] Veigel C and Schmidt C F 2011 Moving into the cell: single-molecule studies of molecular motors in complex environments *Nat. Rev. Mol. Cell Biol.* **12** 163–76
- [32] Vilfan A, Frey E, Schwabl F, Thormählen M, Song Y-H and Mandelkow E 2001 Dynamics and cooperativity of microtubule decoration by the motor protein kinesin J. Mol. Biol. 312 1011–26
- [33] Vuijk H D, Rens R, Vahabi M, MacKintosh F C and Sharma A 2015 Driven diffusive systems with mutually interactive Langmuir kinetics *Phys. Rev.* E 91 032143